Astrophys Space Sci
DOI 10.1007/s10509-014-1886-y

ORIGINAL ARTICLE

Atmospheric models of He-peculiar stars: synthetic He I line profiles and absolute visual magnitudes

Rodolfo Vallverdú · Lydia Cidale · René Rohrmann · Adela Ringuelet

Received: 18 February 2013 / Accepted: 15 March 2014
© Springer Science+Business Media Dordrecht 2014

Abstract We analyze the influence of magnetic pressure effects on the atmospheric structure of B peculiar type stars, as well as, on the emergent He I line profiles and absolute visual magnitudes.

We consider a photosphere in local thermodynamic and hydrostatic equilibrium. The hydrostatic equilibrium equation is modified to include the Lorentz force. Atomic occupational numbers are computed in LTE considering non-ideal effects in the gas equation of state.

We depict the influence of a magnetic field on local He I line profiles and discuss the effects of the helium abundance in magnetic B-type stars. The Lorentz force might explain local variations up to 7 % in the equivalent width of helium lines, while local enhancements of He chemical abundances would produce larger changes. To analyze the line variations in real stars we computed the net contribution of a bipolar magnetic field over the stellar disk. The resulting disk-averaged magnetic field predicts variations with the rotation phase up to 2–3 % in the line EWs for a dipolar magnetic field of 1000 G.

R. Vallverdú (✉) · L. Cidale · A. Ringuelet
Departamento de Espectroscopía, Facultad de Ciencias Astronómicas y Geofísicas, Universidad Nacional de La Plata (UNLP), Paseo del Bosque S/N, B1900FWA La Plata, Argentina
e-mail: rodolfo@fcaglp.unlp.edu.ar

R. Vallverdú · L. Cidale
Instituto de Astrofísica de La Plata, CCT-La Plata, CONICET-UNLP, Paseo del Bosque S/N, B1900FWA La Plata, Argentina

R. Rohrmann
ICATE-CONICET, Av. España Sur 1512, J5402DSP San Juan, Argentina

Published online: 29 March 2014

Keywords Stars: magnetic field · Stars: chemically peculiar · Stars: early-type · Stars: atmospheres · Line: profiles

1 Introduction

Chemically peculiar (CP) stars comprise a particular group of slow rotators B-F type stars that show abnormal abundance enhancements or deficiencies of some chemical species in their atmospheres (Jaschek and Jaschek 1987). This group includes not only the classical Am (A metal) and Ap (A peculiar) stars but also the Hg-Mn and He-weak stars. Among these subgroups, it is possible to distinguish a non-magnetic sequence that includes the Am and Hg-Mn stars as well as a magnetic sequence consisting of Ap stars and some He-weak stars (Preston 1974). Besides the classical group of CP stars, we find the He-strong stars which are considered the high-temperature extension of Ap/Bp (B peculiar) stars (Osmer and Peterson 1974).

Some Ap/Bp stars have strong variable magnetic fields (up to tens of kG) with typical periods of a few days (Bohlender et al. 1987; Borra et al. 1983) while others, with weak magnetic fields, often host a magnetic field stronger than about 300 G. Aurière et al. (2007) interpreted this apparent field strength threshold as a critical field strength, below which magnetic fields are unstable to rotational distortion.

Magnetic early-type stars show photometric and spectroscopic variations that correlate with the rotation period. This phenomenon is interpreted in terms of the Oblique Rotator Model (ORM, Stibbs 1950). In this scenario, as the star rotates, a magnetic dipolar field tilted with respect to the rotation axis changes its orientation relative to an external observer, and its interaction with gravitational and radiative

diffusion processes would give rise to a non-uniform chemical distribution on the stellar surface. Moreover, large-scale diffusion and/or toroidal electric currents may distort the original dipolar magnetic configuration and lead to a significant surface Lorentz force (LeBlanc et al. 1994). The presence of a vertical magnetic force may change the structure of the atmosphere (Stępień 1978; Carpenter 1985) influencing the distribution of chemical composition and contributing to the observed light variations. Furthermore, the existence of non force-free fields may give fundamental clues to understand the origin and the evolution of the stellar magnetic field topology.

The effect of the Lorentz force has been theoretically studied among the Ap stars by Carpenter (1985), LeBlanc et al. (1994), Valyavin et al. (2004), and observationally reported in the works of Kroll (1989), Valyavin et al. (2005) and Shulyak et al. (2007). Although the magnetic configuration of late-Bp stars can be statistically described by the superposition of a dipolar and a non-linear quadripolar field orientated arbitrarily (Bagnulo et al. 2002), similar to the case of the Ap stars, the effect of the Lorentz force has been little studied. Recently, it has been shown that a model with the outward-directed Lorentz force in a dipolar + quadripolar configuration is likely to reproduce the variations observed in the H lines of the late-Bp star 56 Ari (Shulyak et al. 2010).

Assuming, then, that magnetic early B-type stars have similar magnetic configurations to their cooler counterparts, we aim to study the contribution of a surface Lorentz force on their atmospheric structure. We will analyze the response of He I line profiles and absolute visual magnitudes to different magnetic field strengths.

Interesting targets to apply this theory are the He-variable stars. Occasionally, these stars can oscillate between a He-weak and He-strong type star, as is the case of HD 125823 (a Cen) (Norris 1968).

In Sect. 2 we solve the equation of hydrostatic equilibrium, including a term that accounts for the magnetic force, to derive distributions of density and opacity with the optical depths. This atmospheric model is used to compute theoretical neutral He line profiles under the assumption of LTE by means of the radiative transfer equation. In Sect. 3 we present the results related to local and disk-integrated lines of He I λ5015 Å and He I λ5876 Å, $(U-B)$ and $(B-V)$ color indexes and absolute visual magnitudes. Finally, Sect. 4 summarizes the main results.

2 The atmospheric model

To compute the atmospheric structure, we basically use the code developed by Rohrmann (2001) and Rohrmann et al. (2002). In this numerical code, hydrogen-helium model atmospheres are calculated under the assumptions of plane-parallel geometry, constant gravity, local thermodynamic equilibrium, constant energy flux, and homogeneous chemical composition. Radiation transfer and energy flux equations are solved by means of a standard linearization technique. Specifically, the equation of radiative transfer (formulated in terms of the variable Eddington factors) and the constant flux condition are solved by means of an iterative procedure over linearized equations for a set of optical depth points and a frequency mesh. Temperature corrections at each depth point are obtained by means of the Rybicki procedure, in which the resulting systems of linear equations are ordered not in depth blocks but in frequency blocks (see Gustafsson and Nissen 1972). Density and pressure structures are evaluated in each numerical iteration by integration of the hydrostatic equilibrium equation. This calculation is improved to analyze the magnetic effects (see Sect. 2.1). The independent variable is the optical depth τ corresponding to the Rosseland mean opacity.

The adopted atomic configuration consists of 100 bound levels for H I and He II and 144 bound levels for He I. Atomic populations are computed within the occupational probability formalism of Hummer and Mihalas (1988) for the treatment of non-ideal effects in the gas equation of state. This formalism avoids typical rough truncations of particle partition functions and gives a thermodynamical self-consistent way for evaluating the ionization and excitation equilibrium in the gas. Specifically, the atomic population numbers, n_i, relative to the total particle density of each species, $n_{\rm tot}$, is given by

$$\frac{n_i}{n_{\rm tot}} = \frac{w_i g_i \exp(-E_i/KT)}{U}, \tag{1}$$

where w_i is the occupational probability of level i, g_i the statistical weight, E_i the excitation energy, U the internal local partition function, K the Boltzmann constant and T the gas temperature. The factors w_i sum up the perturbations of atomic levels due to neutral and charged particles by taking into account the finite size of species with bound electrons and the effects of the electric field arising from ions and electrons. In particular, charge effects are based on a fit to quantum mechanical Stark ionization theory (Nayfonov et al. 1999).

2.1 Magnetic pressure effects

In order to account for the presence of a magnetic field the Lorentz force term, $f_{\rm l}$, is included in the hydrostatic equilibrium equation, following the procedure proposed by Valyavin et al. (2004),

$$\nabla P = \rho\vec{g} + \vec{f_{\rm l}} = \rho\vec{g} + \frac{1}{c}\vec{j}\times\vec{B}, \tag{2}$$

where $\vec{B}$ is the total magnetic field and $\vec{j}$ is the induced electric current. In a plane-parallel geometry, this equation can be written as:

$$\frac{\partial P}{\partial r} = -\rho g_{\rm eff}. \tag{3}$$

where $g_{\rm eff}$ is an effective gravity, that considers the presence of the Lorentz force which is defined as:

$$g_{\rm eff} = g \pm \sum_i \frac{\lambda_i \sin\theta}{c\rho(1+(\omega_i\tau_i)^2)} E_{\rm eq} B_\theta, \tag{4}$$

where the summation is performed over all the charged particle species i. Here, λ_i is the electrical conductivity; $\omega_i = q|B|/m_i$, is the cyclotron frequency for particle of mass m_i; τ_i is the time associated to the free main-path of the particles; $E_{\rm eq}$ is the electric field at the equator; B_θ is the θ component of the magnetic field and θ is the co-latitude angle; c is the speed of light; ρ the mass density.

This formalism assumes a dipolar magnetic structure and neglects the Hall effect.

To solve the hydrostatic equation, first, we compute temperature and density distributions for a non-magnetic case assuming that the surface gravity is constant for all optical depths. This atmospheric structure gives the initial conditions to calculate the structure of the atmosphere of a magnetic star. Our model atmospheric code is improved to compute the electrical conductivity, the Lorentz force and the variation of effective gravity with depth. To determine the electrical conductivity we adopt the formalism described by Valyavin et al. (2004), Shulyak et al. (2007) and Shulyak et al. (2010). Then, the effective gravity is determined via Eq. (4) and the hydrostatic equilibrium equation is solved including the Lorentz force. The new density distribution is used to improved the calculation of the electrical conductivity and $g_{\rm eff}$. The iteration scheme is repeated until the convergence of $g_{\rm eff}$ is achieved. Typically, it is necessary around 6 or 7 iterations to obtain a percent discrepancy of 0.1 % in $\log g_{\rm eff}$.

To test our atmospheric model we compute electron and ion electrical conductivity (Fig. 1, upper panel) and the effective gravity (Fig. 1, lower panel) as function of the Rosseland mean optical depth for a star with $T_{\rm eff} = 11{,}000$ K, $B_{\rm eq}$ strengths of 200, 500, and 1000 G, and an inward-directed Lorentz force. Our results agree good with those obtained by Valyavin et al. (2004). The discrepancies found between the electrical conductivities derived from both atmospheric models are small. Instead, the comparison of the curves of $g_{\rm eff}/g$ ratios with optical depths obtained in this work with those derived by Valyavin et al. (2004) show discrepancies (up to 15 %, for weak magnetic field strengths) in the outer parts of the atmosphere. These discrepancies could be due to the neglect of metals in our model atmospheres and resulting errors in the temperature structure.

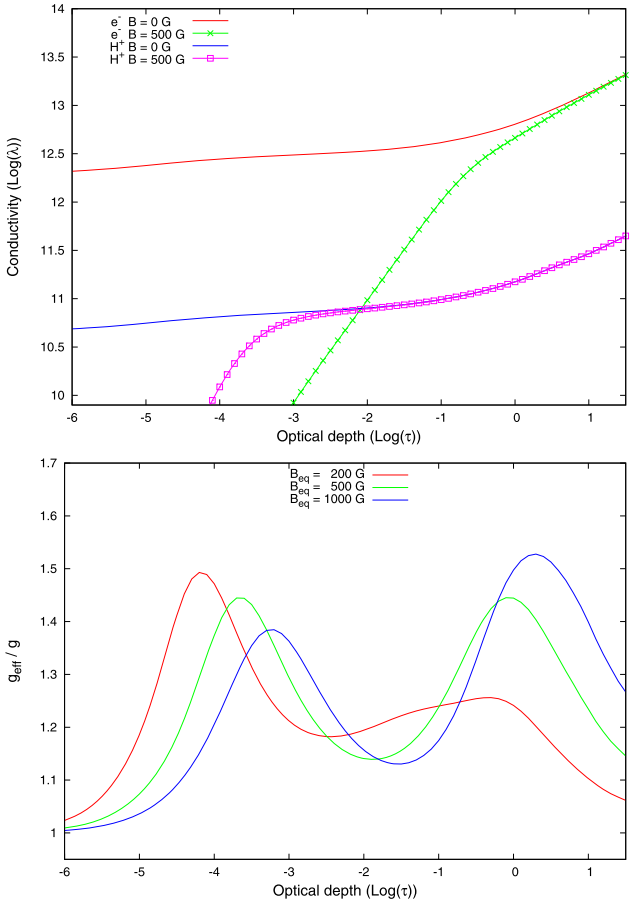

Fig. 1 Distribution of the electrical conductivity (*upper panel*) and effective gravity (*lower panel*) vs. the Rosseland mean optical depth for a stellar model with $T_{\rm eff} = 11{,}000$ K, equatorial magnetic field strengths ($B_{\rm eq}$) of 200, 500, and 1000 G and the Lorentz force directed inwards. The behavior of the curves resemble those obtained by Valyavin et al. (2004)

Finally, we compute the emergent radiation in the He I lines by means of the radiative transfer equation and analyze the effects of the magnetospheric structure (new density and temperature distributions) on the line profiles.

3 Results

In the present study we calculate equator model magnetospheres for different intensities of the magnetic field, ranging from 0 to 2000 G, for either an inward-directed or outward-directed Lorentz force to analyze local effects on the line emergent profiles. We also study disk-averaging effects of the magnetic field with the rotation phase.

We choose stellar parameters corresponding mainly to a typical He-strong object: $T_{\rm eff} = 22{,}000$ K, $\log g = 4$. We find that an equatorial strength of the induced electric field of $\sim 5 \times 10^{-11}$ cm$^{-1/2}$ g$^{1/2}$ s^{-1} seems to be enough to obtain substantial differences in the stellar atmospheric density structure.

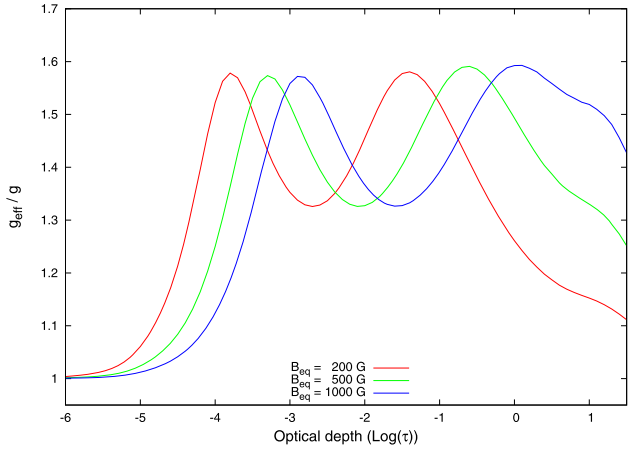

Fig. 2 Variation of the effective gravity vs. the Rosseland mean optical depth for a star with $T_{\rm eff} = 22{,}000$ K and magnetic field strengths ($B_{\rm eq}$) of 200, 500, and 1000 G with the Lorentz force directed inwards

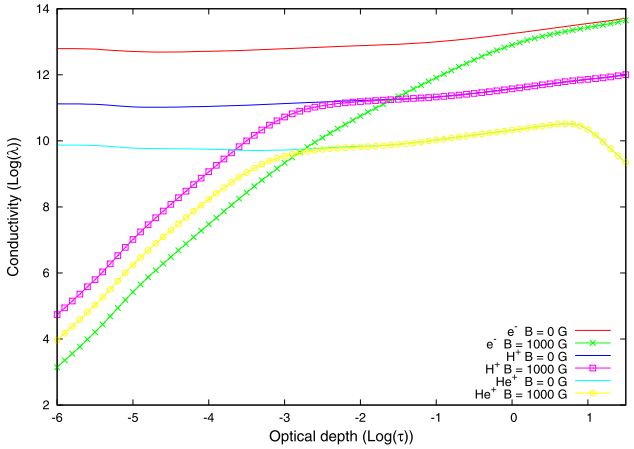

Fig. 3 Variation of the conductivity vs. the optical depth for electrons, H II and He II, in absence of a magnetic field and a polar magnetic field strength of 1000 G. The Lorentz force is inward-directed

Figure 2 shows the variation of the computed effective gravity (normalized to the surface gravity in the absence of a magnetic field) with the Rosseland mean optical depth for an inward-directed Lorentz force with $B_{\rm eq}$ strengths: 200, 500, and 1000 G. Models computed with the Lorentz force directed outwards yield mirror images to the ones shown in the figure.

The effective gravity for an inward-directed (outward-directed) Lorentz force shows two relative maxima (minima) almost equals at different depth depending on the intensity of the magnetic field. The enhancements of the effective gravity, and therefore of the gas pressure, occurs deeper in the atmosphere as the magnetic field strength increases. In the innermost regions, this enhancement is related to the increment of the time associated to the free main-path of the electrons, and the recovering of $g_{\rm eff}$ towards the unity is due to the drop of the electron electrical conductivity (see Fig. 3). The second variation of the effective gravity with depth is dominated by H and He free main-path times and their corresponding electrical conductivities.

It is interesting to stress that the behavior of the effective gravity with the optical depth depends on the magnetic field strength and on the effective temperature of the star, as can be observed when comparing the ratios $g_{\rm eff}/g$ in stars with $T_{\rm eff} = 11{,}000$ K and $T_{\rm eff} = 22{,}000$ K, respectively (see Fig. 1, lower panel, and Fig. 2).

3.1 Local He I line profiles

The effective gravity may change drastically the local atmospheric structure of magnetic stars and, hence, the intensity of the absorption lines. This effect is larger when the magnetic force is directed outwards (Stępień 1978). Then, to quantify the effect of a magnetic non-free force we compute local synthetic He I line profiles for different magnetic field strengths.

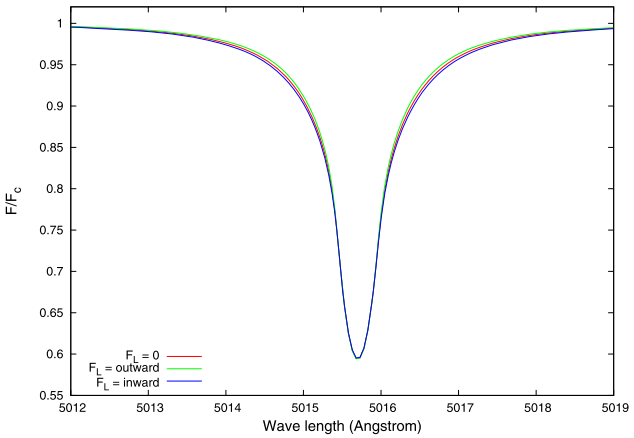

Fig. 4 Normalized line profiles of He I λ5015 with magnetic field strength equal to 0 and 1000 G and both directions of the Lorentz force

The He I λ5015 and λ5876 lines have been treated as Voigt profiles which combine the Doppler broadening due to thermal motions and the Stark effect with broadening parameters (electron-, proton-, and ionized helium-impact line widths and shifts) of Dimitrijevic and Sahal-Brechot (1990). The fine structure of the He I λ5876 line[1] is calculated by accounting the J-splitting of the energy level $2\,^3$P with intensities weighted according to their statistical weights, in ratios 1:3:5. However, as sub-levels $2\,^3P_1$ and $2\,^3P_2$ have also similar energies, the resulting profile consists of two Voigt profiles, of appropriate Doppler widths and shifts, and a line intensity weighted by a factor of 1/8 relative to the main component (Bethe and Salpeter 1957; Shipman and Strom 1970).

Figures 4 and 5 show the resulting He I profiles for $B_{\rm eq} = 1000$ G and the Lorentz force directed either inwards or

[1] The energy levels of the state ^{3}D practically are coincident.

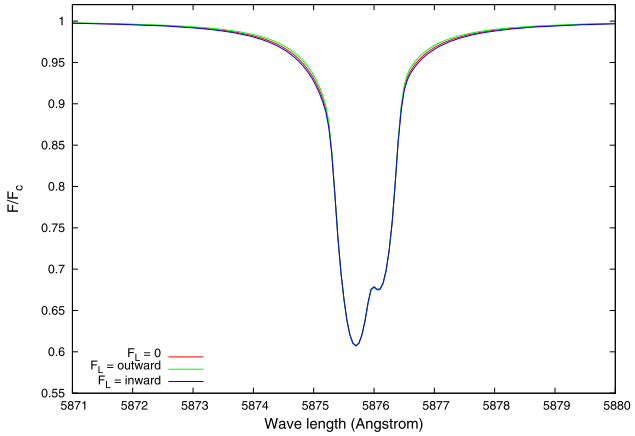

Fig. 5 Normalized line profiles of He I λ5876 with magnetic field strength equal to 0 and 1000 G and both directions of the Lorentz force

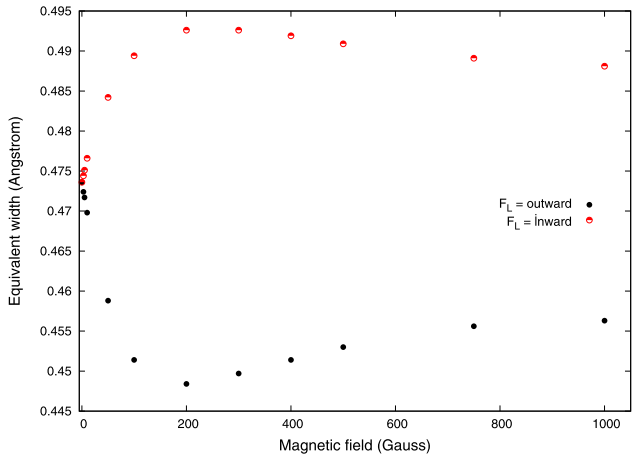

Fig. 6 Line equivalent width of He I λ5015 Å for different intensities of the local magnetic field

outwards. A model without a magnetic field is also plotted. As the variations on a local line profile are very small and depend on the magnetic strength, the calculation of the line equivalent width (EW) as a function of B_{eq} provides a better representation. Figure 6 displays this behavior for the line He I λ5015 Å. The line EW increases when the Lorentz force is outward-directed, otherwise decreases. The maximum variation in the line EW is observed for weak magnetic fields (around 200 G) and an outwards-directed Lorentz force, while for strong magnetic fields the line EW trends to a constant value. The result shown in Fig. 6 gives an idea of the behavior of the He I lines among similar stars with different magnetic field strengths.

We find that the expected local variation in the line equivalent width between a magnetic configuration with the Lorentz force inward-directed and outward-directed is about 7 %. However, due to the large errors present in the line EWs estimates when fitting the continuum level, Valyavin et al. (2004) proposed the use of the residual line profile which results by the subtraction of a line profile from a another chosen as a reference. Figures 7 and 8 show residual line profiles corresponding to He I λ5015 Å and He I λ5876 Å obtained by subtracting the line profiles computed for a magnetic and non-magnetic case. It is possible to observe that the magnetic pressure affects mainly the line wings. The sign of the residual line flux in the wings (positive or negative) is determined by the direction of the local Lorentz force (outward- or inward-directed).

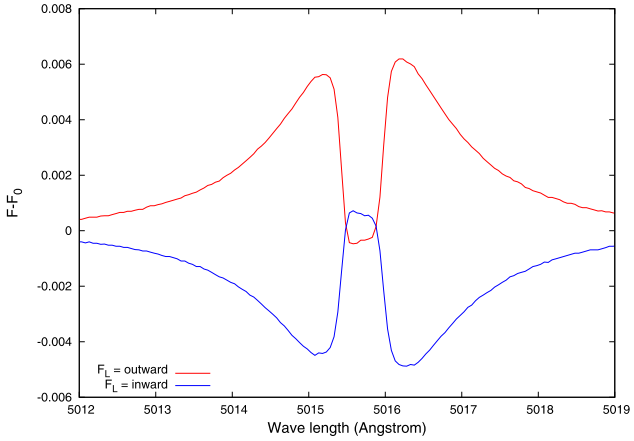

Fig. 7 The He I λ5015 line. Residual line profiles obtained by subtracting the line profiles for a photospheric model with and without a magnetic field considering an outward- and inward-directed Lorentz force

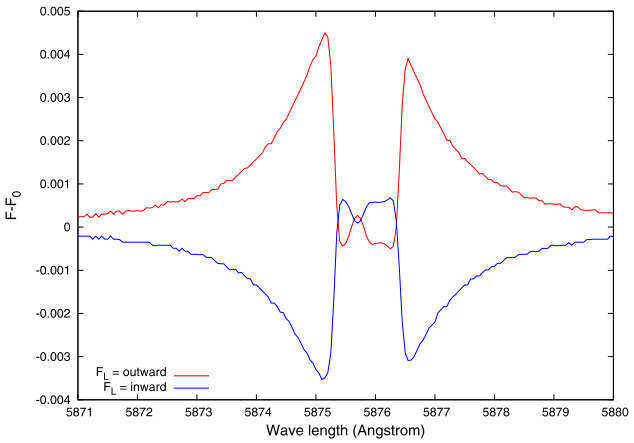

Fig. 8 The He I λ5876 line. Difference between the line profiles for a photospheric model with and without a magnetic field considering an outward- and inward-directed Lorentz force

3.2 Absolute visual magnitudes

Table 1 shows absolute visual magnitudes and color indexes obtained for different B_{eq} field strengths. Local variations in the continuum flux level originated by an outward- and inward-directed force are very small (e.g, ∼0.005 mag). This means that the Lorentz force has its largest influence

Table 1 Absolute visual magnitudes and color indexes computed for a B2 V star with 22,000 K and log $g = 4$ and different B_{eq} strengths

B_{eq}	Outward Lorentz force			Inward Lorentz force		
	M_v	$B-V$	$U-B$	M_v	$B-V$	$U-B$
1000	−2.414	−0.230	−0.912	−2.409	−0.228	−0.907
500	−2.415	−0.230	−0.913	−2.409	−0.228	−0.907
100	−2.413	−0.229	−0.913	−2.410	−0.228	−0.907
50	−2.412	−0.229	−0.912	−2.411	−0.229	−0.908
0	−2.411	−0.229	−0.909	−2.411	−0.229	−0.909

on the physical properties of the upper photospheric layers where the lines form.

3.3 Disk-integrated line profiles

As a consequence of the stellar rotation and the relative orientation of a magnetic dipole with the rotation axis, both g_{eff} and the Lorentz force are expected to change through the stellar surface modifying the local atmospheric structure and, therefore, the appearance of the emergent line profiles. In a stellar rotation cycle we may observe different aspects of the magnetosphere of the star: the equatorial zone, where the Lorentz force has its maximum value or the polar region where the magnetic force vanishes. Thus, to calculate the net contribution of the magnetic force on the observed line profile we need to take into account disk-averaging effects. To this aim we computed magnetospheric models in which the density structure is calculated considering disk-integrated projections of the tangential field component onto the magnetic axis $\langle B_\theta \sin\theta \rangle$, the field modulus $\langle B \rangle$ and its longitudinal component $\langle B_z \rangle$ for different rotation phases, as is described in Valyavin et al. (2004, see Sect. 6.2). Figure 9 shows these magnetic parameters, as function of the rotation phase, for a dipolar magnetic field $B_p = 1000$ G, an inclination angle $i = 90°$, a magnetic obliquity $\beta = 90°$ and a limb-darkening coefficient $\mu = 0.4$. The resulting disk-integrated EWs of He I λ5015 and He I λ5876 lines as function of the rotation phase for an inward-directed Lorentz force are shown in Fig. 10. The maximum difference (∼2 %) is found at phases 0.25 or 0.75 with respect to phases 0 or 0.5 for the line He I λ5015 Å. This variation is lower that the one expected for a local line profile. In the case of an outward-directed Lorentz force the difference is a bit larger (about 3 %) and the maximum value in the line EW occurs at phases 0 or 0.5.

The analysis of disk-integrated visual magnitudes and color indexes do not show detectable variations with the rotation phase.

3.4 Enhanced chemical abundances on line profiles

In Sect. 3.1 we showed that the effect produced by a magnetic non-free force on the local emergent line profile is small, and found that this contribution is even lower when disk-averaging effects are taken into account. However, magnetic fields may favor gravitational diffusion processes and produce chemical abundance fluctuations (Underhill et al. 1975), originating local enhancements/deficiencies in helium. Hence, we compute the helium line radiation for different He/H ratio (see Fig. 11). We found that the linear increment in the line EWs of He I λ5015 Å increases a factor 3 when N_{He}/N_H enhances between 0.03 to 0.25. Thus, the resulting variation is an order of magnitude larger than that expected from the local effects produced by the Lorentz force. This result suggests calculating more sophisticated models combining effects of the magnetic configurations and regions with enhanced or deficient He abundance, which is beyond the goals of the present paper.

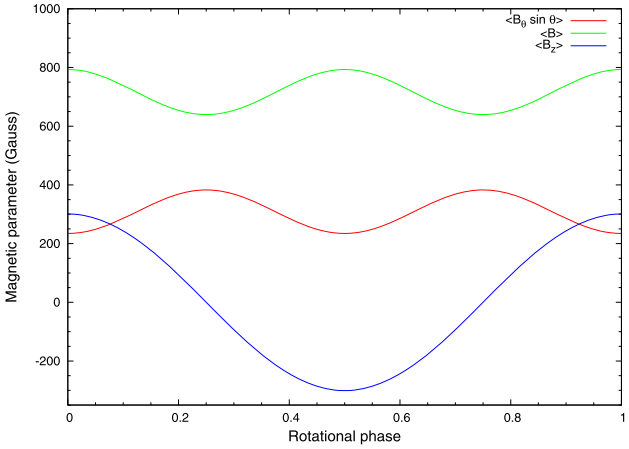

Fig. 9 Disk-integrated projections of $\langle B_\theta \sin\theta \rangle$, $\langle B \rangle$ and $\langle B_z \rangle$ for a bipolar magnetic field $B_p = 1000$ G, $i = 90°$, and $\beta = 90°$ with the rotation phase. We assume a limb-darkening coefficient of 0.4

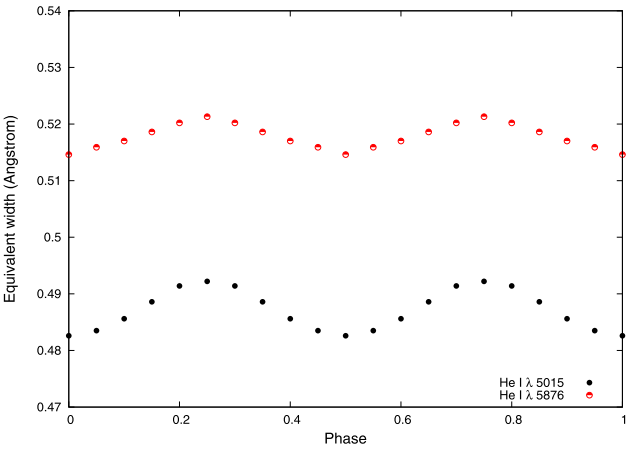

Fig. 10 Variation of the He I line equivalent widths with phase corresponding to the disk-averaged magnetic fields shown in Fig. 9 and an inward-directed Lorentz force

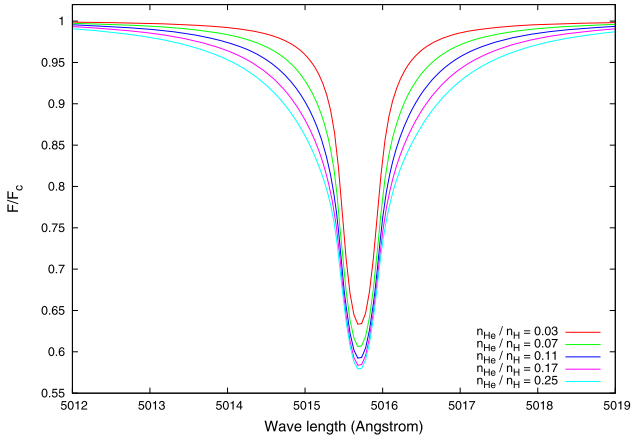

Fig. 11 Variation in the line profile of He I λ5015 due to different He abundances

Table 2 Absolute visual magnitudes and color indexes for different He/H ratios in absence of a magnetic field

N_{He}/N_H	M_V	$B-V$	$U-B$
0.03	−2.386	−0.240	−0.886
0.07	−2.399	−0.234	−0.898
0.11	−2.411	−0.229	−0.909
0.17	−2.425	−0.223	−0.922
0.25	−2.439	−0.218	−0.937

3.5 Effects of chemical abundances on absolute magnitudes

From a theoretical analysis, Cidale et al. (2007) showed that an enhancement of the ratio He/H modifies the Balmer discontinuity and the spectral distribution yielding to an overestimate of the effective temperature. The higher the He/H ratio the smaller the Balmer discontinuity and the brighter the Paschen continuum. Therefore, the stellar atmospheres of B stars become less opaque due to the transparency of He I in the visible continuum and the reduction of the relative number of H absorbing atoms. The effect of different surface helium abundances for a non-magnetic configuration is summarized in Table 2 where the differences in the visual absolute magnitudes and color indexes due to the extreme values of He/H ratio are ∼0.05 dex, an order of magnitude larger than the local variations expected from the effects of a magnetic pressure (see Table 1).

4 Discussion and conclusions

To study the influence of a non-collinear and non-force free magnetic field in the atmospheric structure of a magnetic B-type star we included the term of the Lorentz force in the hydrostatic equilibrium equation. An iterative calculation was employed to derive the temperature and density distributions as well as the electron and ion electrical conductivities. For the treatment of perturbations of neutral and/or charge particles we considered, in particular, non-ideal effects in the gas equation of state. Finally, absolute visual magnitudes and synthetic He I line profiles were obtained by means of the radiative transfer equation in the LTE approximation.

We found that magnetic pressure effects can produce local variations in the EWs of He I λ5015 and λ5876 lines up to 7 % between a magnetic configuration with the Lorentz force inward- and outward-directed. However, the dependence of the Lorentz force with latitude makes the star to exhibit atmospheric regions with different physical properties. The Lorentz force is expected to be maximum at the magnetic equator and zero at the magnetic poles. Therefore, in a rotation period, the star may exhibit variations in the longitudinal component of the magnetic field due to the particular orientation of the magnetic field with respect to the rotation axis. When the magnetic obliquity is near 90° maximum (positive) and minimum (negative) values of the effective magnetic field are equal. The net contribution of a bipolar magnetic field, as a result of disk-averaging effects and a limb darkening, on the EWs of He I lines is very low, leading to line EW variations with the rotation phase up to 2–3 %.

In this work, we also analyzed local effects of helium abundance enhancements/deficiencies on the line profile and continuum fluxes. We found that the local effects originated by changes in the chemical abundances are more relevant than those expected from the Lorentz force.

The effect of the Lorentz force is described in this work via the induced electric field at the equator. In order to calculate this force we adopted a free value for E_{eq} and equal to $5 \times 10^{-11}\,\mathrm{cm}^{-1/2}\,\mathrm{g}^{1/2}\,\mathrm{s}^{-1}$. Nevertheless, we tested with other ranges of this parameter. Lower E_{eq} values have no influence on the atmospheric structure, while large E_{eq} values could lead to unstable solutions (i.e., an $E_{eq} \sim 10^{-10}\,\mathrm{cm}^{-1/2}\,\mathrm{g}^{1/2}\,\mathrm{s}^{-1}$ increases the effective surface gravity in a factor of 5). However, the adopted value can be compared with the induced electric field produced by the global field decay of a dipolar fossil magnetic field and a rough estimate of this value could give clues about its origin. Then, considering the observations of magnetic fields of a few kG (Petit et al. 2013) and assuming that stable configurations of the global stellar magnetic field exist for B strength larger than 300 G (Aurière et al. 2007), we calculate $E_{eq} \sim R_* B_0/ct$ for $B_0 \sim 1$ kG, $R_* = 5.2 R_\odot$, and a characteristic decay time for the magnetic field of $t \sim 3.3 \times 10^9$ years ($t \sim 4\pi\sigma_i R^2/c^2$ with $\sigma_i = 5.6 \times 10^{13}$ CGS units, Landstreet 1987), we obtain $E_{eq} \sim 1.2 \times 10^{-13}\,\mathrm{cm}^{-1/2}\,\mathrm{g}^{1/2}\,\mathrm{s}^{-1}$. This value is two orders of magnitude lower than the E_{eq} necessary to produce magnetic pressure effects in the atmospheric

structure. Therefore, different mechanisms should be taken into account to produce significant atmospheric currents in Ap/Bp stars, as it is discussed in Shulyak et al. (2010).

Acknowledgements We thank the anonymous Referee whose acute criticisms and valuable suggestions helped us to improve the current version of this paper. R.V. also wants to express his gratitude to Dr. A.M. Platzeck for very helpful discussions on magnetic fields in astrophysical plasmas. This research was partially supported by grants from Agencia Nacional de Promoción Científica y Tecnológica (Préstamo BID PICT 2011/0885), CONICET (PIP 0300) and the Programa de Incentivos (G11/109) of the Universidad Nacional de La Plata.

References

Aurière, M., Wade, G.A., Silvester, J., Lignières, F., Bagnulo, S., Bale, K., Dintrans, B., Donati, J.F., Folsom, C.P., Gruberbauer, M., Hui Bon Hoa, A., Jeffers, S., Johnson, N., Landstreet, J.D., Lèbre, A., Lueftinger, T., Marsden, S., Mouillet, D., Naseri, S., Paletou, F., Petit, P., Power, J., Rincon, F., Strasser, S., Toqué, N.: Astron. Astrophys. **475**, 1053 (2007). arXiv:0710.1554. doi:10.1051/0004-6361:20078189

Bagnulo, S., Landi Degl'Innocenti, M., Landolfi, M., Mathys, G.: Astron. Astrophys. **394**, 1023 (2002)

Bethe, H.A., Salpeter, E.E.: Quantum Mechanics of One- and Two-electron Atoms. Dover, New York (1957)

Bohlender, D.A., Landstreet, J.D., Brown, D.N., Thompson, I.B.: Astrophys. J. **323**, 325 (1987)

Borra, E.F., Landstreet, J.D., Thompson, I.: Astrophys. J. Suppl. Ser. **53**, 151 (1983)

Carpenter, K.G.: Astrophys. J. **289**, 660 (1985)

Cidale, L.S., Arias, M.L., Torres, A.F., Zorec, J., Frémat, Y., Cruzado, A.: Astron. Astrophys. **468**, 263 (2007). arXiv:0705.0541. doi:10.1051/0004-6361:20066454

Dimitrijevic, M.S., Sahal-Brechot, S.: Astron. Astrophys. Suppl. Ser. **82**, 519 (1990)

Gustafsson, B., Nissen, P.E.: Astron. Astrophys. **19**, 261 (1972)

Hummer, D.G., Mihalas, D.: Astrophys. J. **331**, 794 (1988). doi:10.1086/166600

Jaschek, C., Jaschek, M.: Book-Review: The Classification of Stars, vol. 74, p. 612 (1987)

Kroll, R.: In: Klare, G. (ed.) Reviews in Modern Astronomy, vol. 2, p. 194 (1989)

Landstreet, J.D.: Mon. Not. R. Astron. Soc. **225**, 437 (1987)

LeBlanc, F., Michaud, G., Babel, J.: Astrophys. J. **431**, 388 (1994). doi:10.1086/174492

Nayfonov, A., Däppen, W., Hummer, D.G., Mihalas, D.: Astrophys. J. **526**, 451 (1999). arXiv:astro-ph/9901360. doi:10.1086/307972

Norris, J.: Nature **219**, 1342 (1968)

Osmer, P.S., Peterson, D.M.: Astrophys. J. **187**, 117 (1974)

Petit, V., Owocki, S.P., Wade, G.A., Cohen, D.H., Sundqvist, J.O., Gagné, M., Maíz Apellániz, J., Oksala, M.E., Bohlender, D.A., Rivinius, T., Henrichs, H.F., Alecian, E., Townsend, R.H.D., ud-Doula, A., MiMeS Collaboration: Mon. Not. R. Astron. Soc. **429**, 398 (2013). arXiv:1211.0282. doi:10.1093/mnras/sts344

Preston, G.W.: Annu. Rev. Astron. Astrophys. **12**, 257 (1974)

Rohrmann, R.D.: Mon. Not. R. Astron. Soc. **323**, 699 (2001). arXiv:astro-ph/0102182

Rohrmann, R.D., Serenelli, A.M., Althaus, L.G., Benvenuto, O.G.: Mon. Not. R. Astron. Soc. **335**, 499 (2002). arXiv:astro-ph/0205084

Shipman, H.L., Strom, S.E.: Astrophys. J. **159**, 183 (1970). doi:10.1086/150301

Shulyak, D., Valyavin, G., Kochukhov, O., Lee, B.-C., Galazutdinov, G., Kim, K.-M., Han, I., Burlakova, T., Tsymbal, V., Lyashko, D.: Astron. Astrophys. **464**, 1089 (2007). arXiv:astro-ph/0612301

Shulyak, D., Kochukhov, O., Valyavin, G., Lee, B.-C., Galazutdinov, G., Kim, K.-M., Han, I., Burlakova, T.: Astron. Astrophys. **509**, 28 (2010). arXiv:0910.0532

Stępień, K.: Astron. Astrophys. **70**, 509 (1978)

Stibbs, D.W.N.: Mon. Not. R. Astron. Soc. **110**, 395 (1950)

Underhill, A.B., Fahey, R.P., Klinglesmith, D.A.: Astrophys. J. **199**, 120 (1975)

Valyavin, G., Kochukhov, O., Piskunov, N.: Astron. Astrophys. **420**, 993 (2004)

Valyavin, G., Kochukhov, O., Shulyak, D., Lee, B., Galazutdinov, G., Kim, K.-M., Han, I.: J. Korean Astron. Soc. **38**, 283 (2005)